Chapter 7

Maps, Strange Attractors, and Chaos

7.1 Maps

Earlier we studied the parametric oscillator $\ddot{x} + \omega^2(t)\, x = 0$, where $\omega(t+T) = \omega(t)$ is periodic. If we define $x_n = x(nT)$ and $\dot{x}_n = \dot{x}(nT)$, then we have

$$\begin{pmatrix} x_{n+1} \\ \dot{x}_{n+1} \end{pmatrix} = A \begin{pmatrix} x_n \\ \dot{x}_n \end{pmatrix} \ , \tag{7.1}$$

where the matrix M is the path ordered exponential

$$A = \mathcal{P} \exp \int_0^T dt\, M(t) \ , \tag{7.2}$$

where

$$M(t) = \begin{pmatrix} 0 & 1 \\ -\omega^2(t) & 0 \end{pmatrix} \ . \tag{7.3}$$

Eqn. 7.1 defines a discrete linear map from phase space to itself.

A related model is described by the *kicked dynamics* of the Hamiltonian

$$H(t) = \frac{p^2}{2m} + V(q)\, K(t) \ , \tag{7.4}$$

where

$$K(t) = \tau \sum_{n=-\infty}^{\infty} \delta(t - n\tau) \tag{7.5}$$

is the kicking function. The potential thus winks on and off with period τ. Note that

$$\lim_{\tau \to 0} K(t) = 1 \ . \tag{7.6}$$

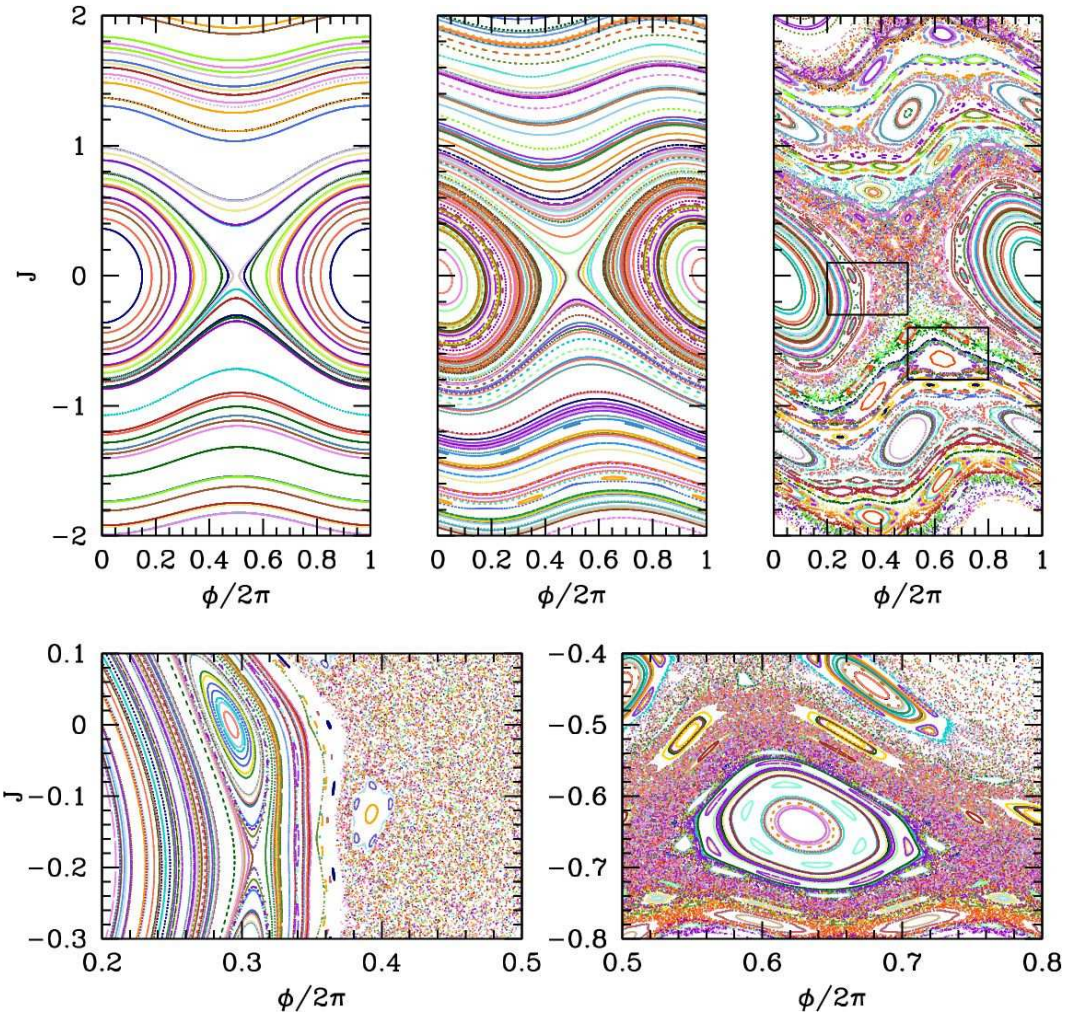

Figure 7.1: Top: the standard map, as defined in the text. Four values of the ϵ parameter are shown: $\epsilon = 0.01$ (left), $\epsilon = 0.2$ (center), and $\epsilon = 0.4$ (right). Bottom: details of the $\epsilon = 0.4$ map.

In the $\tau \to 0$ limit, the system is continuously kicked, and is equivalent to motion in a time-independent external potential $V(q)$.

The equations of motion are

$$\dot{q} = \frac{p}{m} \qquad , \qquad \dot{p} = -V'(q)\, K(t) \ . \tag{7.7}$$

Integrating these equations, we obtain the map

$$q_{n+1} = q_n + \frac{\tau}{m}\, p_n \tag{7.8}$$

$$p_{n+1} = p_n - \tau\, V'(q_n) \ . \tag{7.9}$$

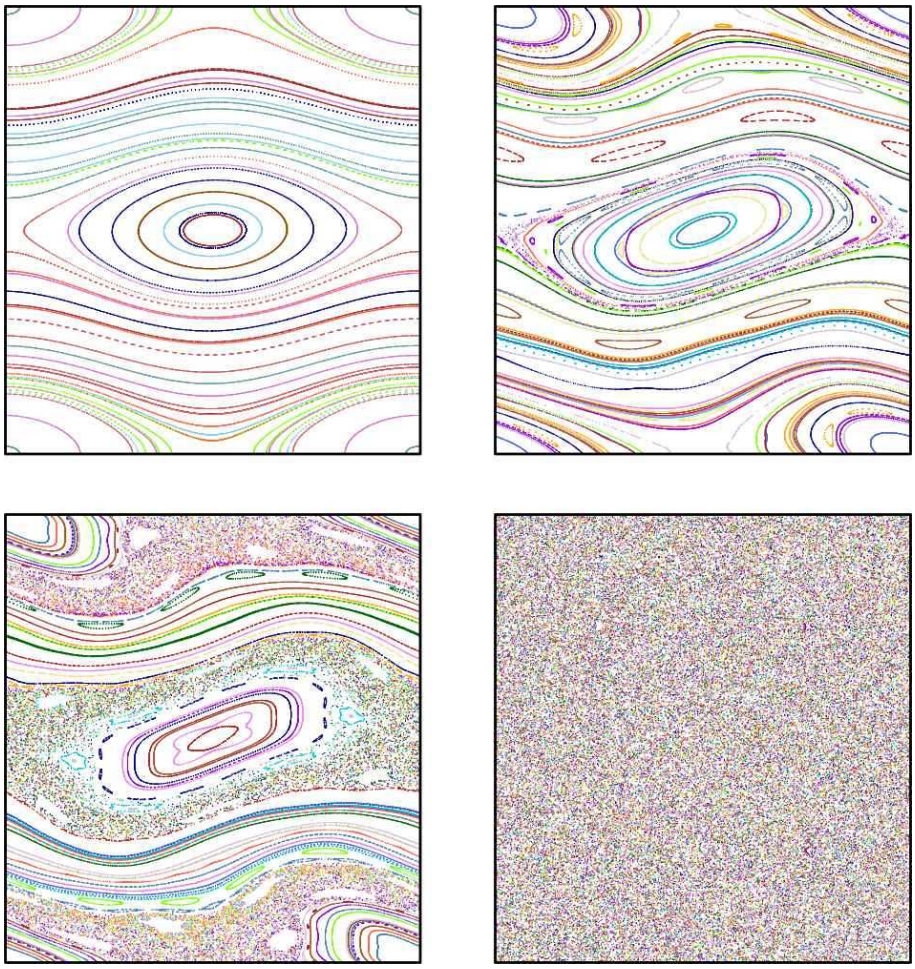

Figure 7.2: The kicked harper map, with $\alpha = 2$, and with $\epsilon = 0.01$, 0.125, 0.2, and 5.0 (clockwise from upper left). The phase space here is the unit torus, $\mathbb{T}^2 = [0,1] \times [0,1]$.

Note that the determinant of Jacobean of the map is unity:

$$\frac{\partial(q_{n+1}\,,\,p_{n+1})}{\partial(q_n\,,\,p_n)} = \begin{pmatrix} 1 & \frac{\tau}{m} \\ -\tau\,V''(q_{n+1}) & 1 - \frac{\tau^2}{m}\,V''(q_{n+1}) \end{pmatrix} \ . \tag{7.10}$$

This means that the map preserves phase space volumes.

Consider, for example, the Hamiltonian $H(t) = \frac{L^2}{2I} - V\cos(\phi)\,K(t)$, where L is the angular momentum conjugate to ϕ. This results in the map

$$\phi_{n+1} = \phi_n + 2\pi\epsilon\,J_n \tag{7.11}$$

$$J_{n+1} = J_n - \epsilon\sin\phi_{n+1}\ , \tag{7.12}$$

where $J_n = L_n/\sqrt{2\pi IV}$ and $\epsilon = \tau\sqrt{V/2\pi I}$. This is known as the *standard map*[1]. In the

[1]The standard map us usually written in the form $x_{n+1} = x_n + \mathcal{J}_n$ and $\mathcal{J}_{n+1} = \mathcal{J}_n - k\sin(2\pi x_{n+1})$. We can recover our version by rescaling $\phi_n = 2\pi x_n$, $\mathcal{J}_n \equiv \sqrt{k}\,J_n$ and defining $\epsilon \equiv \sqrt{k}$.

limit $\epsilon \to 0$, we may define $\dot{x} = (x_{n+1} - x_n)/\epsilon$ and $\dot{J} = (J_{n+1} - J_n)/\epsilon$, and we recover the continuous time dynamics $\dot{\phi} = 2\pi J$ and $\dot{J} = -\sin\phi$. These dynamics preserve the energy function $E = \pi J^2 - \cos\phi$. There is a separatrix at $E = 1$, given by $J(\phi) = \pm\frac{2}{\pi}\big|\cos(\phi/2)\big|$. We see from fig. 7.1 that this separatrix is the first structure to be replaced by a chaotic fuzz as ϵ increases from zero to a small finite value.

Another well-studied system is the *kicked Harper model*, for which

$$H(t) = -V_1 \cos\left(\frac{2\pi p}{P}\right) - V_2 \cos\left(\frac{2\pi q}{Q}\right) K(t) \ . \tag{7.13}$$

With $x = q/Q$ and $y = p/P$, Hamilton's equations generate the map

$$x_{n+1} = x_n + \epsilon\,\alpha\,\sin(2\pi y_n) \tag{7.14}$$

$$y_{n+1} = y_n - \frac{\epsilon}{\alpha}\,\sin(2\pi x_{n+1}) \ , \tag{7.15}$$

where $\epsilon = 2\pi\tau\sqrt{V_1 V_2}/PQ$ and $\alpha = \sqrt{V_1/V_2}$ are dimensionless parameters. In this case, the conserved energy is

$$E = -\alpha^{-1}\cos(2\pi x) - \alpha\cos(2\pi y) \ . \tag{7.16}$$

There are then two separatrices, at $E = \pm(\alpha - \alpha^{-1})$, with equations $\alpha\cos(\pi y) = \pm\sin(\pi x)$ and $\alpha\sin(\pi y) = \pm\cos(\pi x)$. Again, as is apparent from fig. 7.2, the separatrix is the first structure to be destroyed at finite ϵ. We shall return to discuss this phenomenon below.

7.2 One-dimensional Maps

Consider now an even simpler case of a purely one-dimensional map,

$$x_{n+1} = f(x_n) \ , \tag{7.17}$$

or, equivalently, $x' = f(x)$. A fixed point of the map satisfies $x = f(x)$. Writing the solution as x^* and expanding about the fixed point, we write $x = x^* + u$ and obtain

$$u' = f'(x^*)\,u + \mathcal{O}(u^2) \ . \tag{7.18}$$

Thus, the fixed point is stable if $\big|f'(x^*)\big| < 1$, since successive iterates of u then get smaller and smaller. The fixed point is unstable if $\big|f'(x^*)\big| > 1$.

Perhaps the most important and most studied of the one-dimensional maps is the logistic map, where $f(x) = rx(1-x)$, defined on the interval $x \in [0,1]$. This has a fixed point at $x^* = 1 - r^{-1}$ if $r > 1$. We then have $f'(x^*) = 2 - r$, so the fixed point is stable if $r \in (1,3)$. What happens for $r > 3$? We can explore the behavior of the iterated map by drawing a *cobweb diagram*, shown in fig. 7.3. We sketch, on the same graph, the curves $y = x$ (in blue) and $y = f(x)$ (in black). Starting with a point x on the line $y = x$, we move vertically until we reach the curve $y = f(x)$. To iterate, we then move horizontally to the line $y = x$

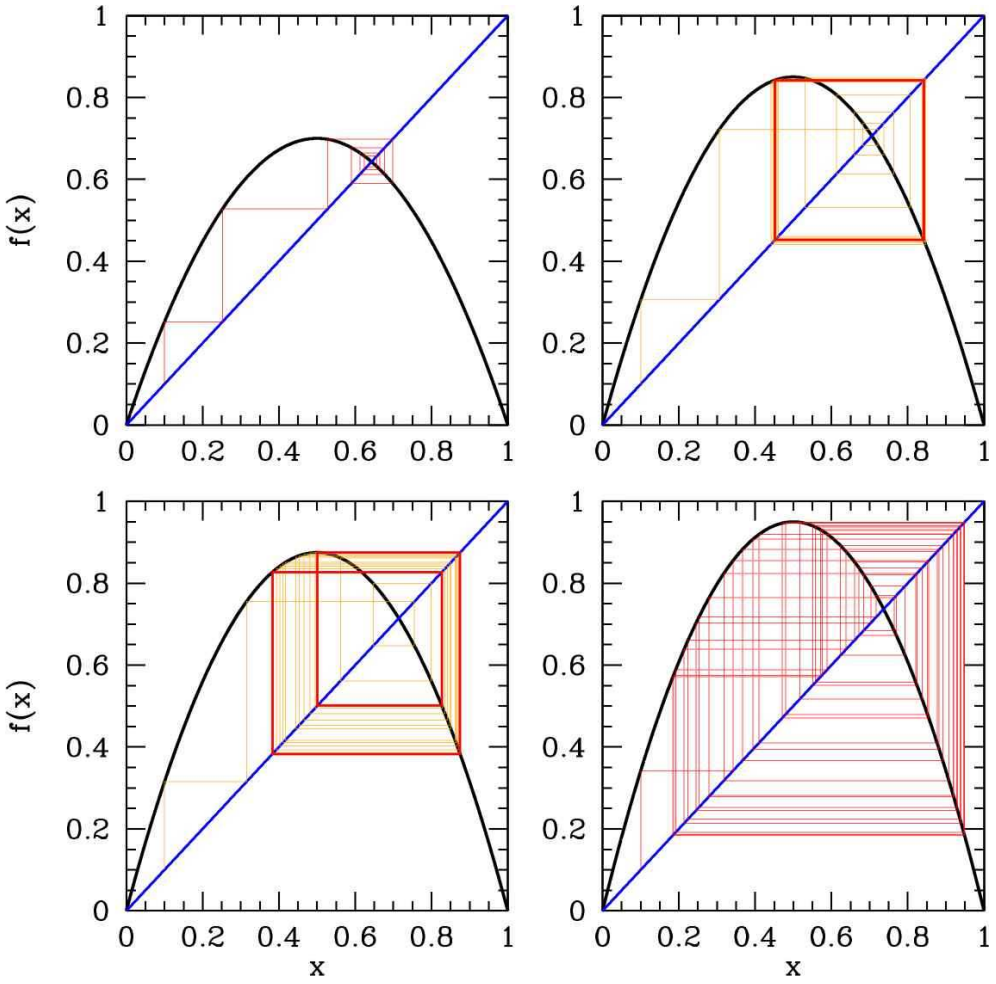

Figure 7.3: Cobweb diagram showing iterations of the logistic map $f(x) = rx(1-x)$ for $r = 2.8$ (upper left), $r = 3.4$ (upper right), $r = 3.5$ (lower left), and $r = 3.8$ (lower right). Note the single stable fixed point for $r = 2.8$, the stable two-cycle for $r = 3.4$, the stable four-cycle for $r = 3.5$, and the chaotic behavior for $r = 3.8$.

and repeat the process. We see that for $r = 3.4$ the fixed point x^* is unstable, but there is a stable two-cycle, defined by the equations

$$x_2 = rx_1(1-x_1) \tag{7.19}$$

$$x_1 = rx_2(1-x_2)\ . \tag{7.20}$$

The second iterate of $f(x)$ is then

$$f^{(2)}(x) = f\big(f(x)\big) = r^2x(1-x)\big(1-rx+rx^2\big)\ . \tag{7.21}$$

Setting $x = f^{(2)}(x)$, we obtain a cubic equation. Since $x - x^*$ must be a factor, we can divide out by this monomial and obtain a quadratic equation for x_1 and x_2. We find

$$x_{1,2} = \frac{1+r \pm \sqrt{(r+1)(r-3)}}{2r}\ . \tag{7.22}$$

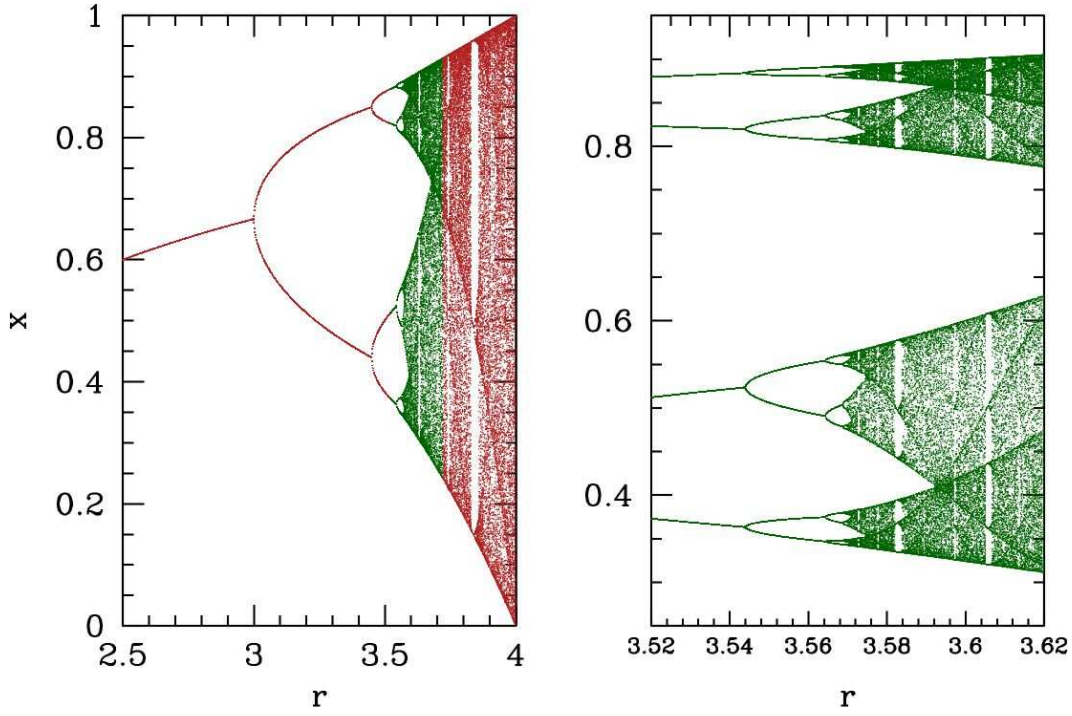

Figure 7.4: Iterates of the logistic map $f(x) = rx(1-x)$.

How stable is this 2-cycle? We find

$$\frac{d}{dx} f^{(2)}(x) = r^2(1-2x_1)(1-2x_2) = -r^2 + 2r + 4 \ . \tag{7.23}$$

The condition that the 2-cycle be stable is then

$$-1 < r^2 - 2r - 4 < 1 \qquad \Longrightarrow \qquad r \in \left[3\,,\,1+\sqrt{6}\right] \ . \tag{7.24}$$

At $r = 1 + \sqrt{6} = 3.4494897\ldots$ there is a bifurcation to a 4-cycle, as can be seen in fig. 7.4.

7.2.1 Lyapunov Exponents

The *Lyapunov exponent* $\lambda(x)$ of the iterated map $f(x)$ at point x is defined to be

$$\lambda(x) = \lim_{n\to\infty} \frac{1}{n} \ln\left(\frac{df^{(n)}(x)}{dx}\right) = \lim_{n\to\infty} \frac{1}{n} \sum_{j=1}^{n} \ln\left(f'(x_j)\right) \ , \tag{7.25}$$

where $x_{j+1} \equiv f(x_j)$. The significance of the Lyapunov exponent is the following. If $\mathsf{Re}\big(\lambda(x)\big) > 0$ then two initial conditions near x will exponentially separate under the iterated map. For the *tent map*,

$$f(x) = \begin{cases} 2rx & \text{if } x < \frac{1}{2} \\ 2r(1-x) & \text{if } x \geq \frac{1}{2} \ , \end{cases} \tag{7.26}$$

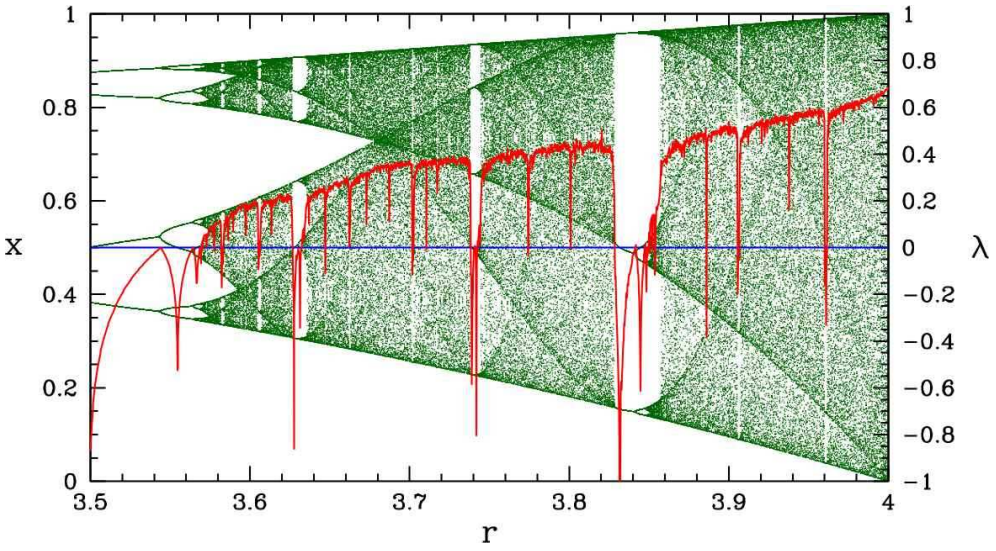

Figure 7.5: Lyapunov exponent for the logistic map.

one easily finds $\lambda(x) = \ln(2r)$ independent of x. Thus, if $r > \frac{1}{2}$ the Lyapunov exponent is positive, meaning that every neighboring pair of initial conditions will eventually separate exponentially under repeated application of the map. The Lyapunov exponent for the logistic map is depicted in fig. 7.5.

7.2.2 Chaos in the logistic map

What happens in the logistic map for $r > 1 + \sqrt{6}$? At this point, the 2-cycle becomes unstable and a stable 4-cycle develops. However, this soon goes unstable and is replaced by a stable 8-cycle, as the right hand panel of fig. 7.4 shows. The first eight values of r where bifurcations occur are given by

$$r_1 = 3 \ , \ r_2 = 1 + \sqrt{6} = 3.4494897 \ , \ r_3 = 3.544096 \ , \ r_4 = 3.564407 \ ,$$
$$r_5 = 3.568759 \ , \ r_6 = 3.569692 \ , \ r_7 = 3.569891 \ , \ r_8 = 3.569934 \ , \ \ldots$$

Feigenbaum noticed that these numbers seemed to be converging exponentially. With the *Ansatz*

$$r_\infty - r_k = \frac{c}{\delta^k} \ , \tag{7.27}$$

one finds

$$\delta = \frac{r_k - r_{k-1}}{r_{k+1} - r_k} \ , \tag{7.28}$$

and taking the limit $k \to \infty$ from the above data one finds

$$\delta = 4.669202 \quad , \quad c = 2.637 \quad , \quad r_\infty = 3.5699456 \ . \tag{7.29}$$

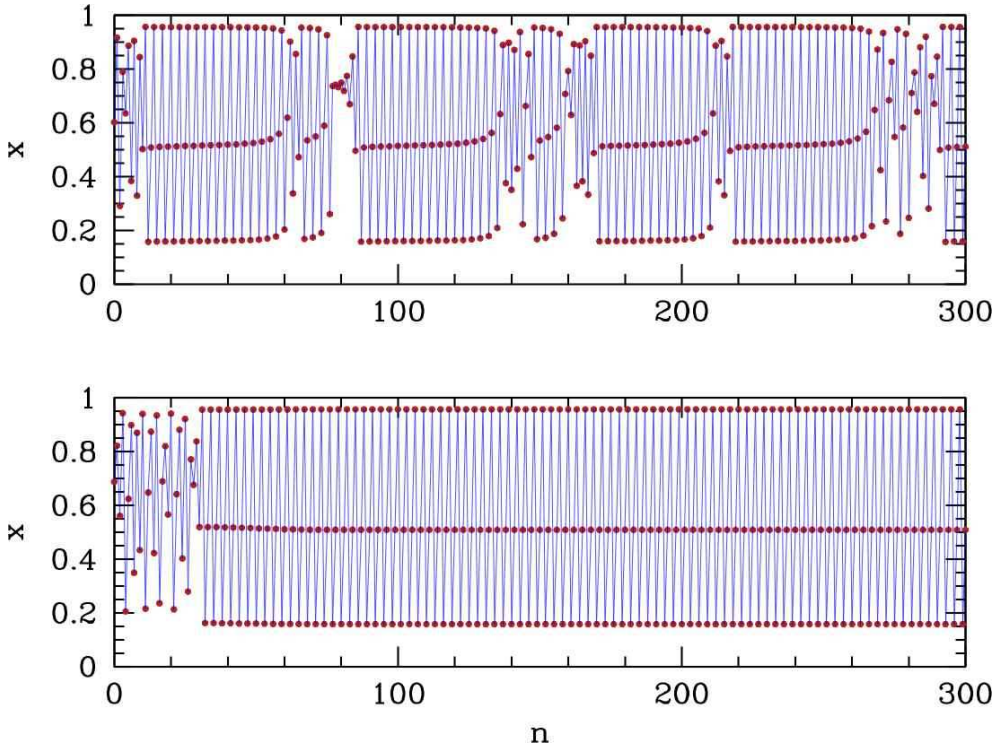

Figure 7.6: Intermittency in the logistic map in the vicinity of the 3-cycle Top panel: $r = 3.828$, showing intermittent behavior. Bottom panel: $r = 3.829$, showing a stable 3-cycle.

There's a very nifty way of thinking about the chaos in the logistic map at the special value $r = 4$. If we define $x_n \equiv \sin^2\theta_n$, then we find

$$\theta_{n+1} = 2\theta_n \ . \tag{7.30}$$

Now let us write

$$\theta_0 = \pi \sum_{k=1}^{\infty} \frac{b_k}{2^k} \ , \tag{7.31}$$

where each b_k is either 0 or 1. In other words, the $\{b_k\}$ are the digits in the binary decimal expansion of θ_0/π. Now $\theta_n = 2^n\theta_0$, hence

$$\theta_n = \pi \sum_{k=1}^{\infty} \frac{b_{n+k}}{2^k} \ . \tag{7.32}$$

We now see that the logistic map has the effect of *shifting* to the left the binary digits of θ_n/π to yield θ_{n+1}/π. The last digit falls off the edge of the world, as it were, since it results in an overall contribution to θ_{n+1} which is zero modulo 2π. This very emphatically demonstrates the sensitive dependence on initial conditions which is the hallmark of chaotic behavior, for eventually two very close initial conditions, differing by $\Delta\theta \sim 2^{-m}$, will, after m iterations of the logistic map, come to differ by $\mathcal{O}(1)$.

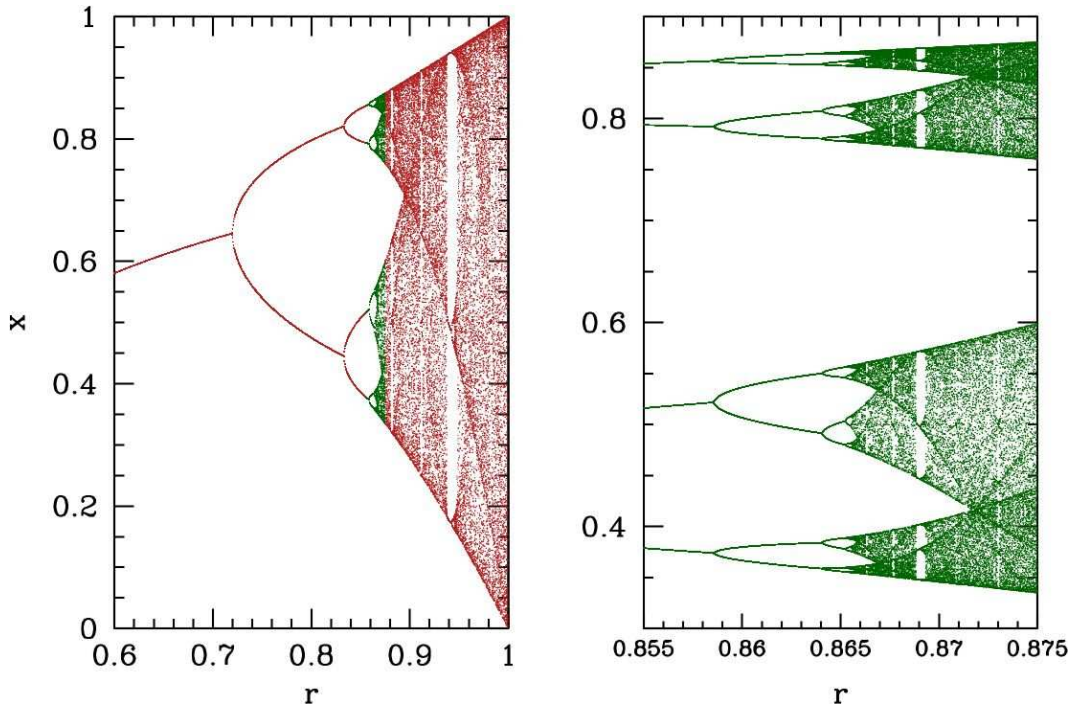

Figure 7.7: Iterates of the sine map $f(x) = r\sin(\pi x)$.

7.2.3 Intermittency

Successive period doubling is one route to chaos, as we've just seen. Another route is *intermittency*. Intermittency works like this. At a particular value of our control parameter r, the map exhibits a stable periodic cycle, such as the stable 3-cycle at $r = 3.829$, as shown in the bottom panel of fig. 7.6. If we then vary the control parameter slightly in a certain direction, the periodic behavior persists for a finite number of iterations, followed by a *burst*, which is an interruption of the regular periodicity, followed again by periodic behavior, *ad infinitum*. There are three types of intermittent behavior, depending on whether the Lyapunov exponent λ goes through $\mathsf{Re}(\lambda) = 0$ while $\mathsf{Im}(\lambda) = 0$ (type-I intermittency), or with $\mathsf{Im}(\lambda) = \pi$ (type-III intermittency, or, as is possible for two-dimensional maps, with $\mathsf{Im}(\lambda) = \eta$, a general real number.

7.3 Attractors

An *attractor* of a dynamical system $\dot{\boldsymbol{\varphi}} = \boldsymbol{V}(\boldsymbol{\varphi})$ is the set of $\boldsymbol{\varphi}$ values that the system evolves to after a sufficiently long time. For $N = 1$ the only possible attractors are stable fixed points. For $N = 2$, we have stable nodes and spirals, but also stable limit cycles. For $N > 2$ the situation is qualitatively different, and a fundamentally new type of set, the *strange attractor,* emerges.

A strange attractor is basically a bounded set on which nearby orbits diverge exponentially (*i.e.* there exists at least one positive Lyapunov exponent). To envision such a set, consider a flat rectangle, like a piece of chewing gum. Now fold the rectangle over, stretch it, and squash it so that it maintains its original volume. Keep doing this. Two points which started out nearby to each other will eventually, after a sufficiently large number of folds and stretches, grow far apart. Formally, a strange attractor is a *fractal*, and may have *noninteger Hausdorff dimension.* (We won't discuss fractals and Hausdorff dimension here.)

7.4 The Lorenz Model

The canonical example of an $N = 3$ strange attractor is found in the Lorenz model. E. N. Lorenz, in a seminal paper from the early 1960's, reduced the essential physics of the coupled *partial* differential equations describing Rayleigh-Benard convection (a fluid slab of finite thickness, heated from below – in Lorenz's case a model of the atmosphere warmed by the ocean) to a set of twelve coupled nonlinear *ordinary* differential equations. Lorenz's intuition was that his weather model should exhibit recognizable patterns over time. What he found instead was that in some cases, changing his initial conditions by a part in a thousand rapidly led to totally different behavior. This *sensitive dependence on initial conditions* is a hallmark of chaotic systems.

The essential physics (or mathematics?) of Lorenz's $N = 12$ system is elicited by the

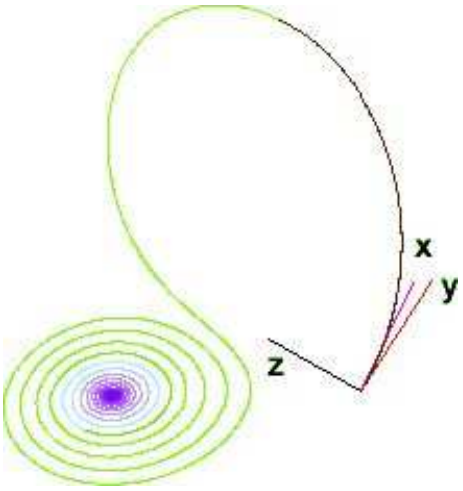

Figure 7.8: Evolution of the Lorenz equations for $\sigma = 10$, $b = \frac{8}{3}$, and $r = 15$, with initial conditions $(x, y, z) = (0, 1, 0)$, projected onto the (x, z) plane. The system is attracted by a stable spiral. (Source: Wikipedia)

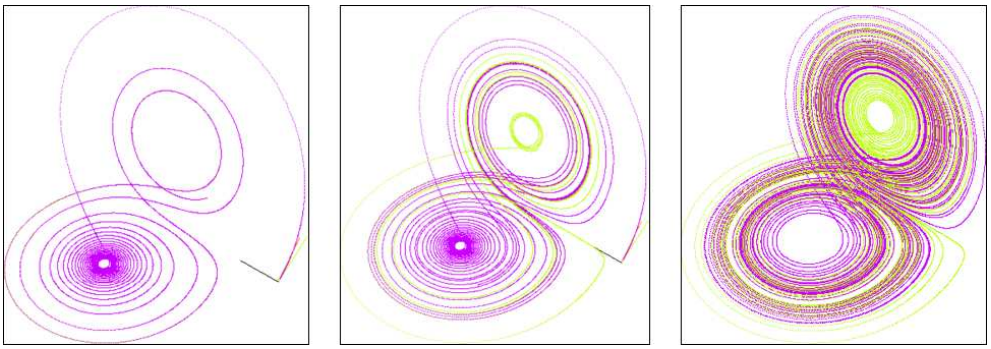

Figure 7.9: Evolution of the Lorenz equations showing sensitive dependence on initial conditions. The magenta and green curves differ in their initial X coordinate by 10^{-5}. (Source: Wikipedia)

reduced $N = 3$ system,

$$\dot{X} = -\sigma X + \sigma Y \tag{7.33}$$

$$\dot{Y} = rX - Y - XZ \tag{7.34}$$

$$\dot{Z} = XY - bZ \ , \tag{7.35}$$

where σ, r, and b are all real and positive. Here t is the familiar time variable (appropriately scaled), and (X, Y, Z) represent linear combinations of physical fields, such as global wind current and poleward temperature gradient. These equations possess a symmetry under $(X, Y, Z) \to (-X, -Y, Z)$, but what is most important is the presence of nonlinearities in the second and third equations.

The Lorenz system is *dissipative* because phase space volumes contract:

$$\boldsymbol{\nabla}\cdot\boldsymbol{V} = \frac{\partial\dot{X}}{\partial X} + \frac{\partial\dot{Y}}{\partial Y} + \frac{\partial\dot{Z}}{\partial Z} = -(\sigma + b + 1) \ . \tag{7.36}$$

Thus, volumes contract under the flow. Another property is the following. Let

$$F(X, Y, Z) = \tfrac{1}{2}X^2 + \tfrac{1}{2}Y^2 + \tfrac{1}{2}(Z - r - \sigma)^2 \ . \tag{7.37}$$

Then

$$\begin{aligned}\dot{F} &= X\dot{X} + Y\dot{Y} + (Z - r - \sigma)\dot{Z} \\ &= -\sigma X^2 - Y^2 - b\big(Z - \tfrac{1}{2}r - \tfrac{1}{2}\sigma\big)^2 + \tfrac{1}{4}b(r + \sigma)^2 \ .\end{aligned} \tag{7.38}$$

Thus, $\dot{F} < 0$ outside an ellipsoid, which means that all solutions must remain bounded in phase space for all times.

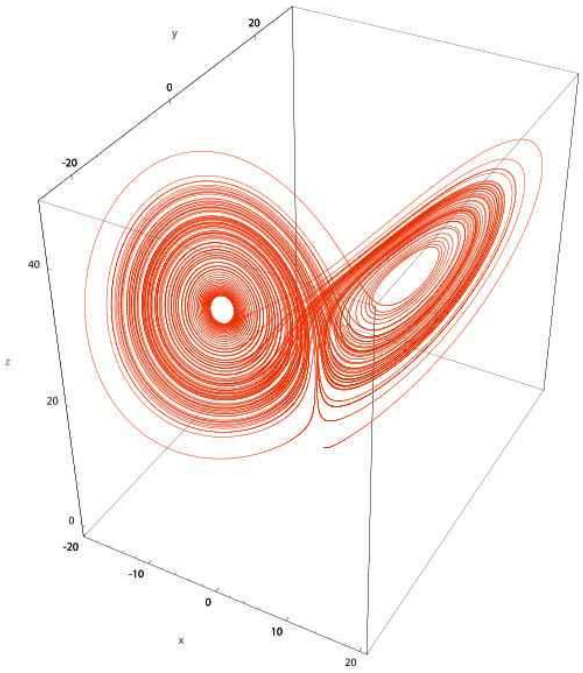

Figure 7.10: Evolution of the Lorenz equations for $\sigma = 10$, $b = \frac{8}{3}$, and $r = 28$, with initial conditions $(X_0, Y_0, Z_0) = (0, 1, 0)$, showing the 'strange attractor'. (Source: Wikipedia)

7.4.1 Fixed point analysis

Setting $\dot{x} = \dot{y} = \dot{z} = 0$, we have three possible solutions. One solution, which is always present, is $x^* = y^* = z^* = 0$. If we linearize about this solution, we obtain

$$\frac{d}{dt}\begin{pmatrix}\delta X\\ \delta Y\\ \delta Z\end{pmatrix} = \begin{pmatrix}-\sigma & \sigma & 0\\ r & -1 & 0\\ 0 & 0 & -b\end{pmatrix}\begin{pmatrix}\delta X\\ \delta Y\\ \delta Z\end{pmatrix} \ . \tag{7.39}$$

The eigenvalues of the linearized dynamics are found to be

$$\begin{aligned}\lambda_{1,2} &= -\tfrac{1}{2}(1+\sigma) \pm \tfrac{1}{2}\sqrt{(1+\sigma)^2 + 4\sigma(r-1)} \\ \lambda_3 &= -b \ ,\end{aligned} \tag{7.40}$$

and thus if $0 < r < 1$ all three eigenvalues are negative, and the fixed point is a stable node. If, however, $r > 1$, then $\lambda_2 > 0$ and the fixed point is attractive in two directions but repulsive in a third, corresponding to a three-dimensional version of a saddle point.

For $r > 1$, a new pair of solutions emerges, with

$$X^* = Y^* = \pm\sqrt{b(r-1)} \quad , \quad Z^* = r - 1 \ . \tag{7.41}$$

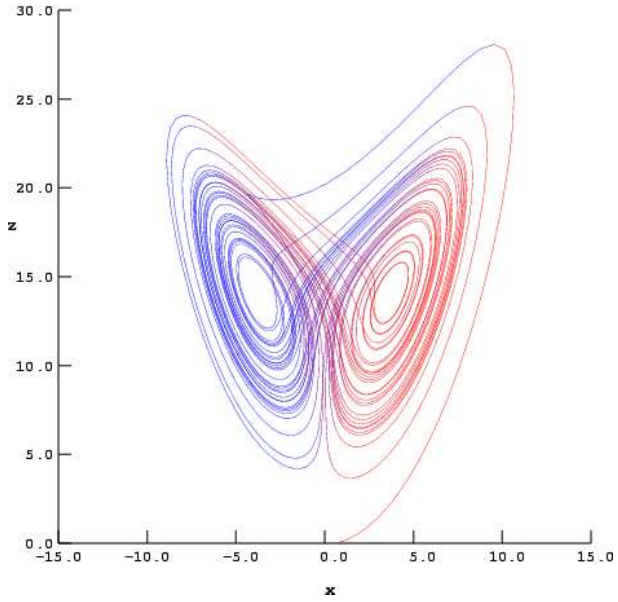

Figure 7.11: The Lorenz attractor, projected onto the (X, Z) plane.

Linearizing about either one of these fixed points, we find

$$\frac{d}{dt}\begin{pmatrix}\delta X\\ \delta Y\\ \delta Z\end{pmatrix} = \begin{pmatrix}-\sigma & \sigma & 0\\ 1 & -1 & -X^*\\ X^* & X^* & -b\end{pmatrix}\begin{pmatrix}\delta X\\ \delta Y\\ \delta Z\end{pmatrix} \ . \tag{7.42}$$

The characteristic polynomial of the linearized map is

$$P(\lambda) = \lambda^3 + (b+\sigma+1)\,\lambda^2 + b(\sigma+r)\,\lambda + 2b(r-1) \ . \tag{7.43}$$

Since b, σ, and r are all positive, $P'(\lambda) > 0$ for all $\lambda \geq 0$. Since $P(0) = 2b(r-1) > 0$, we may conclude that there is always at least one eigenvalue λ_1 which is real and negative. The remaining two eigenvalues are either both real and negative, or else they occur as a complex conjugate pair: $\lambda_{2,3} = \alpha \pm i\beta$. The fixed point is stable provided $\alpha < 0$. The stability boundary lies at $\alpha = 0$. Thus, we set

$$P(i\beta) = \Big[2b(r-1) - (b+\sigma+1)\beta^2\Big] + i\Big[b(\sigma+r) - \beta^2\Big]\beta = 0 \ , \tag{7.44}$$

which results in two equations. Solving these two equations for $r(\sigma, b)$, we find

$$r_{\rm c} = \frac{\sigma(\sigma+b+3)}{\sigma-b-1} \ . \tag{7.45}$$

The fixed point is stable for $r \in \big[1, r_{\rm c}\big]$. These fixed points correspond to steady convection. The approach to this fixed point is shown in Fig. 7.8.

The Lorenz system has commonly been studied with $\sigma = 10$ and $b = \frac{8}{3}$. This means that the volume collapse is very rapid, since $\boldsymbol{\nabla}\cdot\boldsymbol{V} = -\frac{41}{3} \approx -13.67$, leading to a volume contraction

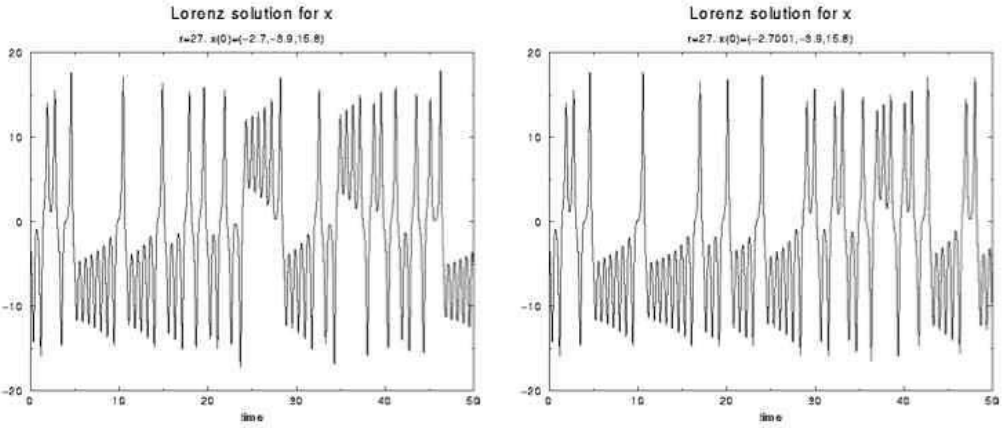

Figure 7.12: $X(t)$ for the Lorenz equations with $\sigma = 10$, $b = \frac{8}{3}$, $r = 28$, and initial conditions $(X_0, Y_0, Z_0) = (-2.7, -3.9, 15.8)$, and initial conditions $(X_0, Y_0, Z_0) = (-2.7001, -3.9, 15.8)$.

of $e^{-41/3} \simeq 1.16 \times 10^{-6}$ per unit time. For these parameters, one also has $r_{\rm c} = \frac{470}{19} \approx 24.74$. The capture by the strange attractor is shown in Fig. 7.10.

In addition to the new pair of fixed points, a strange attractor appears for $r > r_{\rm s} \simeq 24.06$. In the narrow interval $r \in [24.06, 24.74]$ there are then *three* stable attractors, two of which correspond to steady convection and the third to chaos. Over this interval, there is also hysteresis. *I.e.* starting with a convective state for $r < 24.06$, the system remains in the convective state until $r = 24.74$, when the convective fixed point becomes unstable. The system is then driven to the strange attractor, corresponding to chaotic dynamics. Reversing the direction of r, the system remains chaotic until $r = 24.06$, when the strange attractor loses its own stability.

7.4.2 Poincaré section

One method used by Lorenz in analyzing his system was to plot its *Poincaré section*. This entails placing one constraint on the coordinates (X, Y, Z) to define a two-dimensional surface Σ, and then considering the intersection of this surface Σ with a given phase curve for the Lorenz system. Lorenz chose to set $\dot{Z} = 0$, which yields the surface $Z = b^{-1}XY$. Note that since $\dot{Z} = 0$, $Z(t)$ takes its maximum and minimum values on this surface; see fig. 7.13. By plotting the values of the maxima Z_N as the integral curve successively passed through this surface, Lorenz obtained results such as those shown in fig. 7.14, which has the form of a one-dimensional map and may be analyzed as such. Thus, chaos in the Lorenz attractor can be related to chaos in a particular one-dimensional map, known as the *return map* for the Lorenz system.

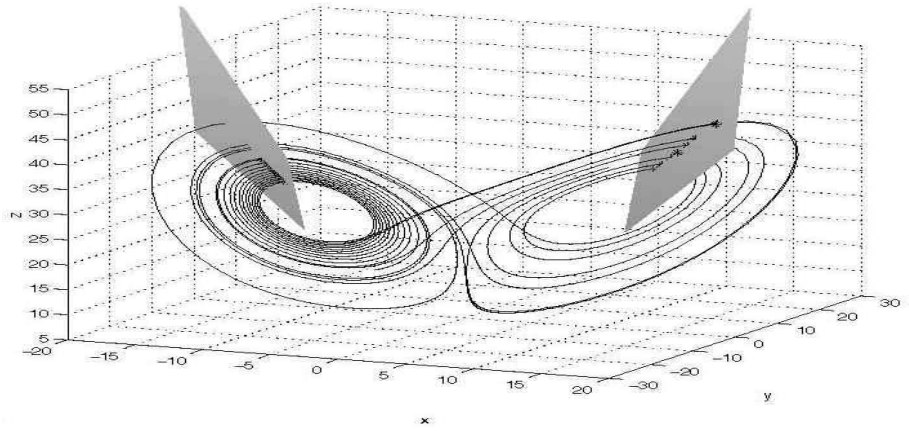

Figure 7.13: Lorenz attractor for $b = \frac{8}{3}$, $\sigma = 10$, and $r = 28$. Maxima of Z are depicted by stars.

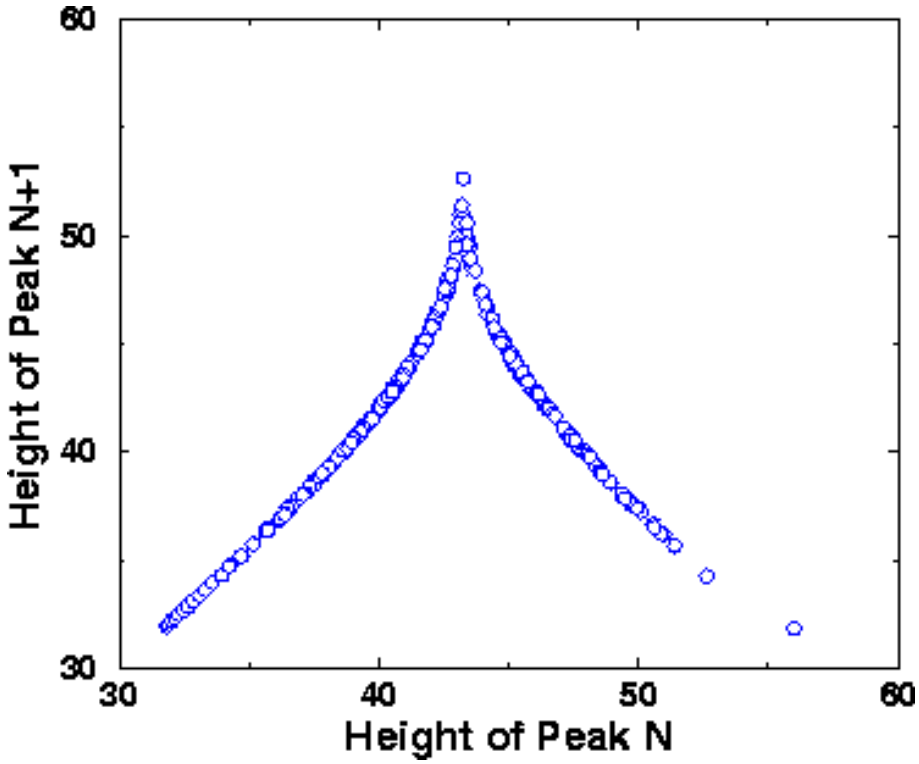

Figure 7.14: Plot of relation between successive maxima Z_N along the strange attractor for the Lorenz system.

7.4.3 Rössler System

Another simple $N = 3$ system which possesses a strange attractor is the Rössler system,

$$\dot{X} = -Y - Z \tag{7.46}$$

$$\dot{Y} = Z + aY \tag{7.47}$$

$$\dot{Z} = b + Z(X - c) \ , \tag{7.48}$$

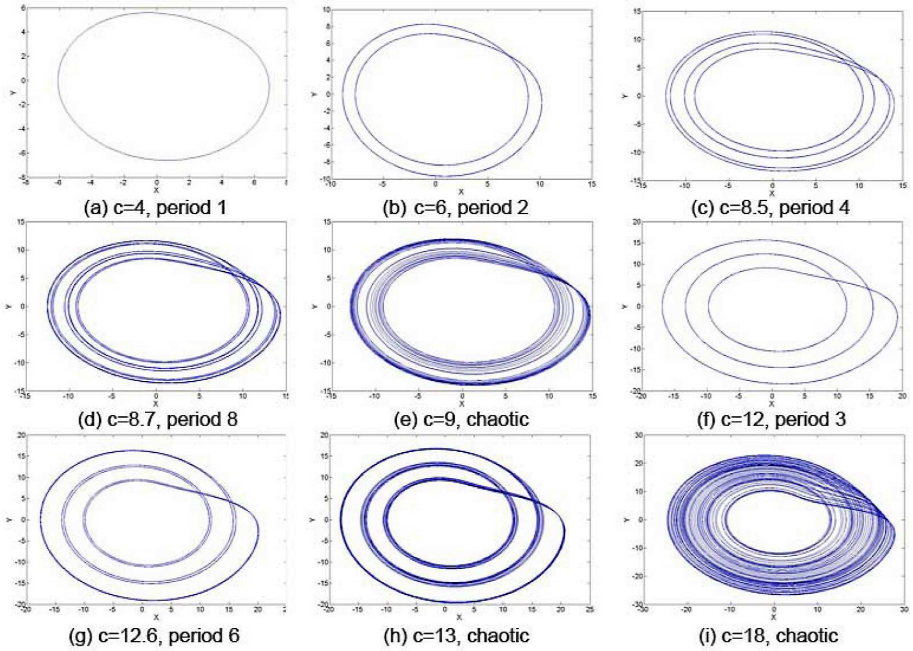

Figure 7.15: Period doubling bifurcations of the Rössler attractor, projected onto the (x, y) plane, for nine values of c, with $a = b = \frac{1}{10}$.

typically studied as a function of c for $a = b = \frac{1}{5}$. In Fig. 7.16, we present results from work by Crutchfield *et al.* (1980). The transition from simple limit cycle to strange attractor proceeds via a sequence of period-doubling bifurcations, as shown in the figure. A convenient diagnostic for examining this period-doubling route to chaos is the *power spectral density,* or PSD, defined for a function $F(t)$ as

$$\Phi_F(\omega) = \left| \int_{-\infty}^{\infty} \frac{d\omega}{2\pi}\, F(t)\, e^{-i\omega t} \right|^2 = \left| \hat{F}(\omega) \right|^2 . \tag{7.49}$$

As one sees in Fig. 7.16, as c is increased past each critical value, the PSD exhibits a series of frequency halvings (*i.e.* period doublings). All harmonics of the lowest frequency peak are present. In the chaotic region, where $c > c_\infty \approx 4.20$, the PSD also includes a noisy broadband background.

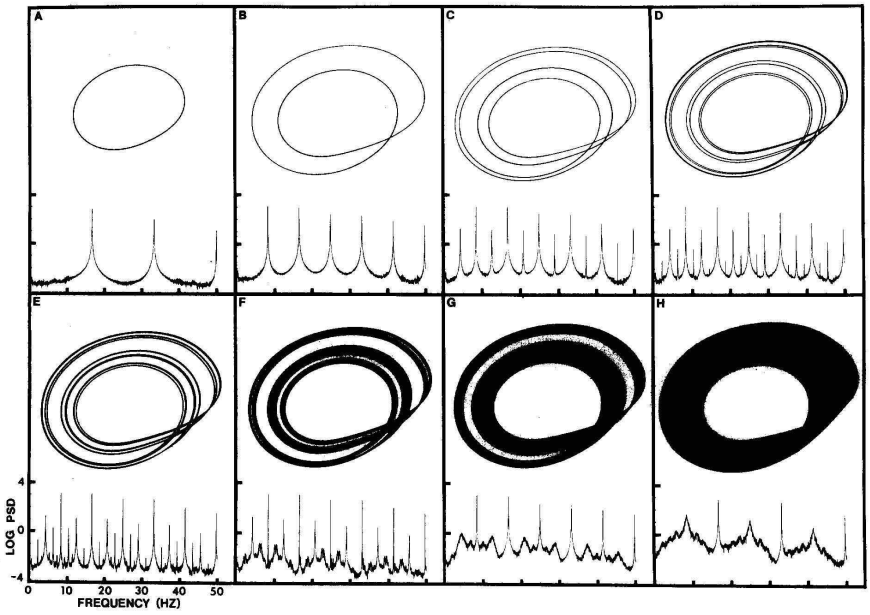

Figure 7.16: Period doubling bifurcations of the Rössler attractor with $a = b = \frac{1}{5}$, projected onto the (X,Y) plane, for eight values of c, and corresponding power spectral density for Z(t). (a) $c = 2.6$; (b) $c = 3.5$; (c) $c = 4.1$; (d) $c = 4.18$; (e) $c = 4.21$; (f) $c = 4.23$; (g) $c = 4.30$; (h) $c = 4.60$.